INDERSCIENCE PUBLISHERS
Linking academia, business and industry through research

International Journal of Machining and Machinability of Materials

ISSN online: 1748-572X - ISSN print: 1748-5711
https://www.inderscience.com/ijmmm

Experimental investigation into electrochemical discharge peripheral surface grinding process of polymer nanocomposites

Nandani Singh, Vinod Yadava, Pragya Shandilya

DOI: 10.1504/IJMMM.2022.10051497

Article History:
Received: 05 July 2022
Accepted: 19 September 2022
Published online: 15 March 2023

Copyright © 2023 Inderscience Enterprises Ltd.

Experimental investigation into electrochemical discharge peripheral surface grinding process of polymer nanocomposites

Nandani Singh*, Vinod Yadava and Pragya Shandilya

Department of Mechanical Engineering,
Motilal Nehru National Institute of Technology Allahabad,
Prayagraj, India
Email: rme1613@mnnit.ac.in
Email: profvinody@gmail.com
Email: pragya20@mnnit.ac.in
*Corresponding author

Abstract: *Polymer nanocomposites*, best possible emerging materials for multifunctional parts/products, are difficult-to-machine due to their enhanced mechanical properties. Electrochemical discharge machining (ECDM) has potential for machining such materials and has been used in configurations like drilling-ECDM, milling-ECDM, TW-ECDM and turning-ECDM. However, limited work has been found in Grinding-ECDM. Therefore, present work attempts to investigate grinding-ECDM. The experiments have been carried out based on one-parameter-at-a-time on indigenously developed experimental setup which has same configuration as conventional peripheral surface grinding; therefore, the process is named as electrochemical discharge peripheral surface grinding (ECDPSG). The effects of supply voltage, pulse-on time, electrolyte concentration, and wheel rotation on MRR and R_a have been analysed during machining of alumina-reinforced-epoxy-nanocomposite. The results show that for MRR, at wheel rotation 3 rpm and 4 rpm, pulse-on time is the dominating parameter, whereas at wheel rotation 5 rpm, supply voltage is the dominating parameter. For R_a, supply voltage is the dominating parameter at all wheel rotations.

Keywords: electrochemical discharge grinding; electrochemical discharge surface grinding; MRR; alumina-reinforced-epoxy-nanocomposites; ARENC; polymer nanocomposites; PNCs.

Reference to this paper should be made as follows: Singh, N., Yadava, V. and Shandilya, P. (2023) 'Experimental investigation into electrochemical discharge peripheral surface grinding process of polymer nanocomposites', *Int. J. Machining and Machinability of Materials*, Vol. 25, No. 1, pp.21–40.

Biographical notes: Nandani Singh is currently pursuing her PhD in Department of Mechanical Engineering at Motilal Nehru National Institute of Technology Allahabad, Prayagraj, India. Her research area focuses on advanced machining.

Vinod Yadava is a Professor in Department of Mechanical Engineering at Motilal Nehru National Institute of Technology Allahabad, Prayagraj, India. He has published many research papers in the reputed international and national journals. He has also been associated with the editorial board of many

Copyright © 2023 Inderscience Enterprises Ltd.

international journals and the national advisory board of many international conferences. He has immense experience in teaching and research consultancy and completed five government-sponsored research projects and ten institute-sponsored research projects. His research interests include hybrid/advanced machining processes, FEM/ANN/DOE applications in manufacturing, laser processing of materials, quality and reliability engineering.

Pragya Shandilya is an Assistant Professor in Department of Mechanical Engineering at Motilal Nehru National Institute of Technology Allahabad, Prayagraj, India. She has published many research papers and book chapters in the reputed international and national journals. Her research interests include advanced machining processes, design and analysis of experiments, rapid prototyping, etc.

1 Introduction

Polymer nanocomposites (*PNCs*) have much more potential over commonly used engineering materials (like ceramics, composites, polymers) due to having improved properties, like electrical non-conductivity and high strength to weight ratio in general, and specifically improved chemical, physical, electrical, and mechanical properties, in particular. These improved properties are due to nano-scale reinforcements (such as nanoplatelets, nanotubes, nanoparticles, and nanofibers) in polymer matrix (Nayak et al., 2022). This is because the nano-reinforcements have higher surface area, therefore their interaction between the polymers matrix is more likely increased. Consequently, the properties like mechanical strength and thermal resistivity enhances multiple of matrix. The practical example of PNC in automotive industry is the application of Nylon 6-clay hybrid (NCH) in timing-belt cover (Kurauchi et al., 1991). In similar manner, PNCs have potential to replace the commonly used engineering materials (like ceramics, composites, polymers) in vast domains of applications like, sport items, aerospace components (Hussain et al., 2006; Zhan et al., 2017), biomedical devices (Duncan, 2015), electrochemical display devices, electric and magnetic shields, electronic packaging, photonic devices (Wing et al., 2003), etc. The advancement conventional machining have disadvantages of removal of nano-scale reinforcements and damaging the workpiece while machining of PNCs (Starost and Njuguna, 2014; Fu et al., 2022). Therefore, there is need to develop an advanced machining process to utilise the utmost advantages of PNCs.

Electrical discharge machining (EDM) has been used for machining electrically conductive PNCs like carbon nano-tubes and graphene used as reinforcement materials; but they are not suitable to machine electrically non-conductive PNCs like inorganic electrically non-conductive nanoparticles as reinforcement materials (Wan et al., 2008). Thus, available literature reveals that electrochemical discharge machining (ECDM) process is suitable to machine PNCs (Yadav et al., 2018, 2020). Different configurations such as drilling-ECDM (Singh et al., 2020), milling-ECDM (Hajian et al., 2018), cutting-ECDM (Yadav et al., 2018), and turning-ECDM (Ali et al., 2019) have been developed to make the variety of features in electrically nonconductive materials. Researchers have modified the existing configurations of ECDM to improve the

performance and make the process more versatile to generate different shapes in difficult-to-machine materials, e.g., ECDM process was used for trepanning of alumina (Chak and Venkateswara Rao, 2007); grinding-ECDM (in face surface mode) was used for machining of metal matrix composites (Liu et al., 2013); grinding aided electrochemical discharge engraving was used to create fluidic channel in borosilicate glass (Ladeesh and Manu, 2018).

Therefore, to explore the capabilities of ECDM process, a peripheral surface grinding feature has been incorporated the existing ECDM configuration. Since, the developed experimental setup has similar configuration to conventional grinding; therefore, the process is named as electrochemical discharge grinding (ECDG) process. ECDG process, utilises a thick metallic disc as tool electrode to remove the workpiece material. Electrochemical action, electric discharge action, and abrasion are responsible for machining in ECDG process. The mechanism of machining can be understood in two part; first, mechanism of spark generation; second, mechanism of material removal. The mechanism of spark generation is similar to the ECDM process. As far as the mechanism of material removal in ECDG process is concerned, it also includes abrasion action with material removal mechanism in ECDM process. Many researchers (Crichton and McGeough, 1985; Basak and Ghosh, 1996; Jain et al., 1999; Kulkarni et al., 2002; Wüthrich and Bleuler, 2004) have tried to explain the mechanism of spark generation. The most acceptable explanation regarding the mechanism of spark generation is percolation theory with tool blanketing. The mechanism of machining in ECDG process is explained in next section.

ECDG process can be configured either on the basis of workpiece and wheel interaction (peripheral and face) or on the basis of workpiece geometry (surface and cylindrical). Hence, in combination, there can be four practically possible configurations of ECDG process: electrochemical discharge peripheral surface grinding (ECDPSG) process, electrochemical discharge face surface grinding (ECDFSG) process, electrochemical discharge peripheral cylindrical grinding (ECDPCG) process, and electrochemical discharge face cylindrical grinding (ECDFCG) process.

The present work is an attempt to develop experimental setup for ECDPSG process, and investigate the performance of the ECDPSG process. The input process parameters, namely, supply voltage, electrolyte concentration, pulse-on time, and wheel rotation are selected whereas output performance parameters like MRR and R_a are selected. MRR was calculated by difference in weight of the workpiece (measured by digital microbalance, accuracy 10 μg, CAS India Private Limited) before and after machining per unit machining time. R_a was measured using surface roughness tester (accuracy 0.1 μm, SURTRONIC-25 model, Taylor Hobson Ltd., UK).

2 Working of ECDPSG process

Figure 1 shows the schematic diagram of ECDPSG process. The wheel here is connected to negative terminal and auxiliary electrode is connected to positive terminal of the pulse DC power supply.

Figure 2 shows the interaction between grinding wheel and workpiece. Electrochemical discharged (ECD) action occurs between bonding material of grinding wheel and electrolyte. There are two essential conditions to observe ECD phenomena. First, the approximate ratio of the immersed surface area of the cathode to anode should

be at least 1:100 (Fascio et al., 2004); and second, the supply voltage should be more than a critical value (minimum voltage required for breakdown of the gas film). When supply voltage reaches to decomposition voltage, electrolysis starts and generates hydrogen gas at the cathode and oxygen gas at the anode. When supply voltage reaches to a critical value, the hydrogen gas film forms around the cathode and isolates it completely from the electrolyte. This gas film works as dielectric (similar to electric discharge machining), and on increasing supply voltage beyond critical value, spark is observed with a high pressure high temperature plasma channel, across the gas film between wheel and electrolyte. The thermal energy produced from this spark is utilised for melting and vaporising the workpiece material, which is placed in the vicinity of cathode. During pulse-off time, when plasma channel collapses the vacuum is created near cathode and electrolyte interface, the molten material moves towards the vacuum and flushed by electrolyte from sparking zone. The re-solidified molten material is removed by abrasion. Hence, in ECDPSG process, material is removed by melting and vaporisation, ejecting and flushing, and by abrasion, simultaneously. Abrasion is possible only by active grains (whose protrusion height more than wheel-workpiece gap).

Figure 1 Schematic diagram of ECDPSG process (see online version for colours)

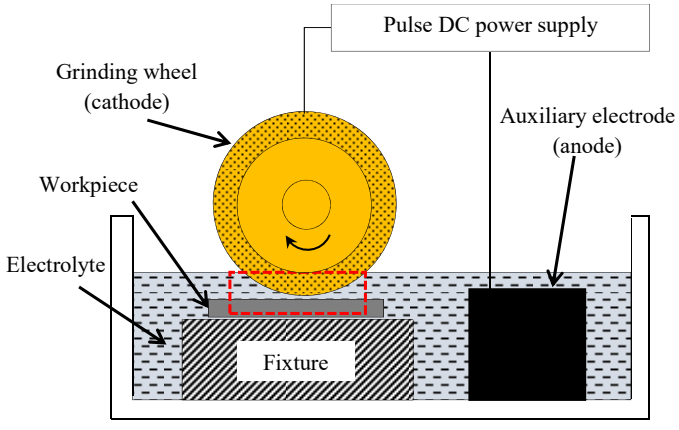

Figure 2 (a) Grinding wheel and workpiece interaction in ECDPSG process (b) Spark generated between grinding wheel and electrolyte (see online version for colours)

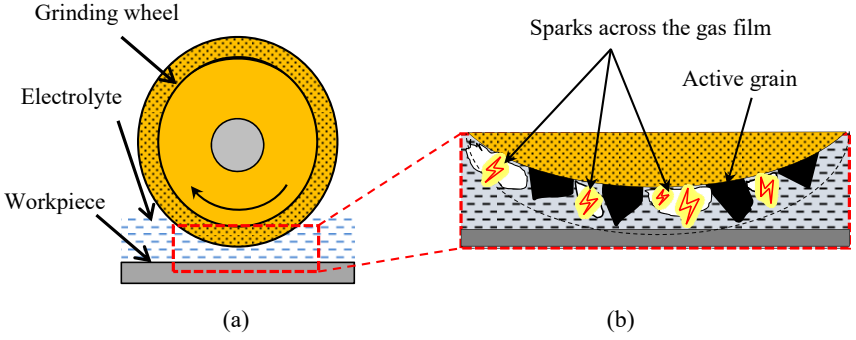

3 Development of experimental setup of ECDPSG process

Basic units of an experimental setup of ECDPSG process: mechanical unit, electrical and electronics unit, and machine user interface are shown in schematic diagram (Figure 3).

Figure 3 Schematic diagram of an experimental setup of ECDPSG process (see online version for colours)

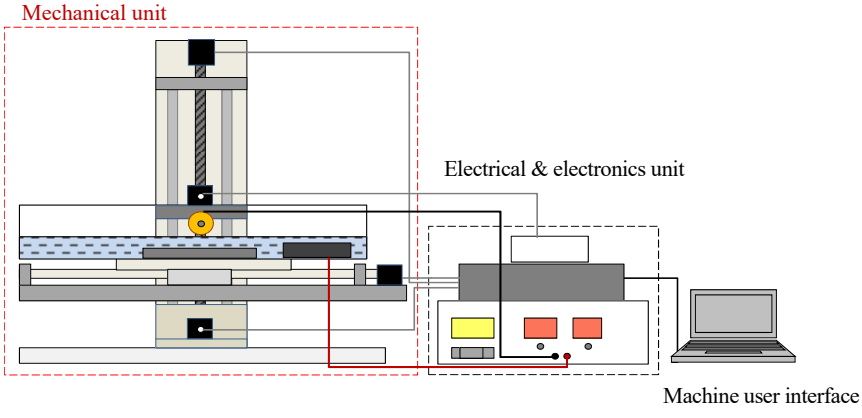

3.1 Mechanical unit

Generally, the mechanical unit consists of the structural components (frame, axles, bearing, fasteners, seals, etc.) and mechanisms (belt-drive and nut-screw). Figure 4 shows the photographic view of the developed mechanical unit of ECDPSG setup consists of worktable, table traversing unit, machining chamber, fixtures, wheel attachment unit, and down feed assembly for the wheel attachment unit. Aluminium, a lightweight material, was selected for the frame, whereas, polypropylene, a chemically inert material, was selected for foundation of machine. The worktable was fixed on the linear sliders and ball screw assembly. Stepper motor provides rotational motion to linear slider and ball screw assembly units. The rpm of the motor is regulated using controller and a machine user program installed on a computer/laptop.

Machining chamber (360 mm × 250 mm × 150 mm) used in experimental setup of ECDPSG process, was made by joining acrylic sheets using screws, and a silicone resin bond, was used to make it leak-proof. The machining chamber was fixed on the worktable. On one side of the machine chamber, a plastic drainage tap was provided to drain the electrolyte after machining. A plastic ruler was attached to monitor the electrolyte level. The polypropylene fixture used in experimental setup of ECDPSG process to hold the workpiece.

Down feed assembly was the linear slider and ball screw assembly and was attached to the vertical frame of the machine. The wheel attachment unit was attached using an L clamp to this down feed assembly. Figure 5 shows the schematic diagram of the wheel attachment unit used in ECDPSG setup. It consists of two square bearing mounts were attached to the bottom of the polypropylene plate to hold the ball bearings. The spindle and bearings were assembled by means of interference fit. To provide the rotary motion to the spindle stepper motor was mounted at the top surface of the polypropylene plate.

The motion was transmitted from the stepper motor to the spindle by pulley and round belt drive. The motion along the z-axis is provided by a similar ball screw linear guide arrangement and stepper motor to the wheel attachment unit.

Figure 4 The photographic view of the mechanical unit of ECDPSG setup (see online version for colours)

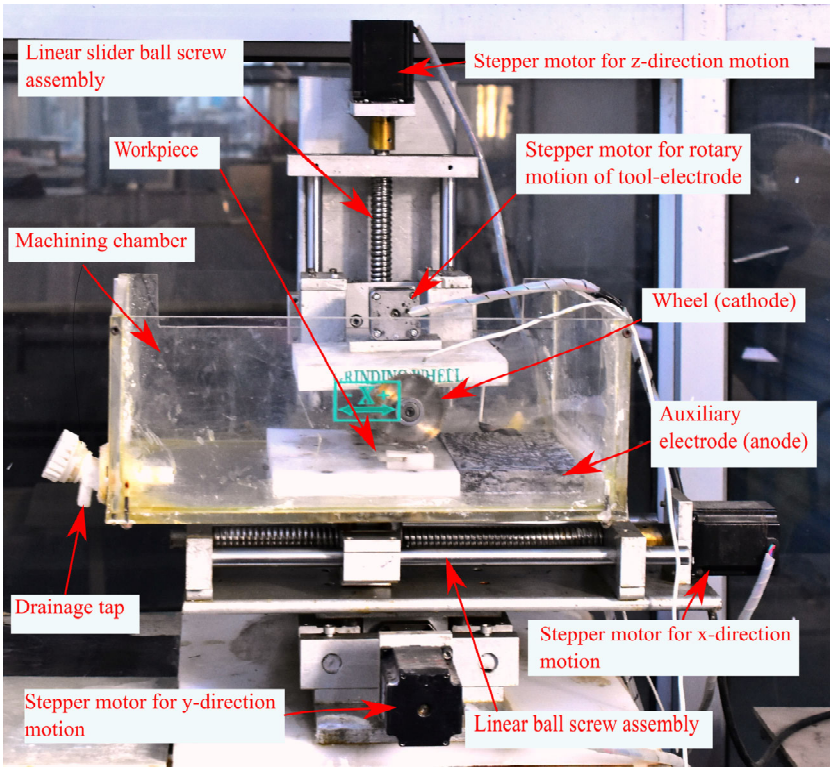

Figure 5 Schematic diagram of wheel attachment unit used in ECDPSG setup

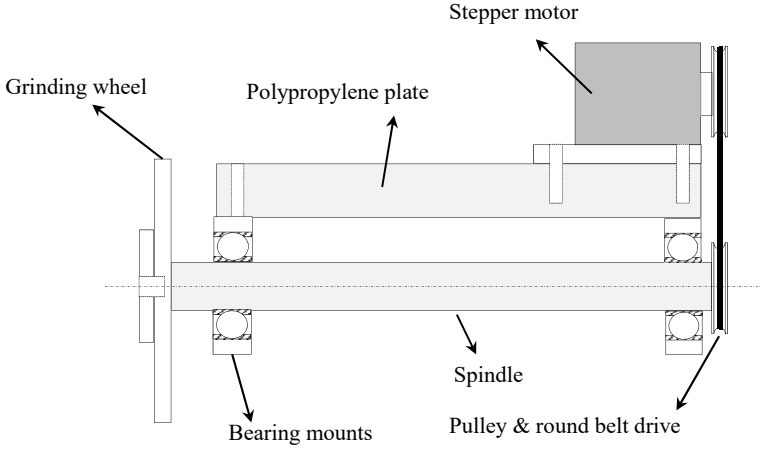

3.2 Electrical and electronic unit

The electrical and electronic unit contains a pulse DC power supply unit and stepper motor controller unit. A pulse DC power supply unit was used to create an electrolytic cell. The negative terminal of the power supply was connected to a wheel, and the positive terminal was connected to the auxiliary electrode (anode). Table 1 shows trials done to select electrodes' materials and geometry to observe spark. Only a few trials were successful in generating the spark, and after these experimental trials final dimensions of electrodes taken in this work, is shown in Table 2. The specifications of electric power supply units, stepper motor controller unit, and machine user interface unit are tabulated in Table 3.

Table 1 Experimental trials and observations

Trial no.	*Specification of cathode and anode*	*Observations*
1	Cathode: Wheel (brass) thickness 5 mm Anode: Graphite rod (diameter 20 mm, length 100 mm)	No spark observed.
2	Cathode: Wheel (brass) thickness 3 mm Anode: Graphite rod (diameter 20 mm, length 100 mm)	No spark observed.
3	Cathode: Metal sheet (copper) thickness 0.27 mm Anode: Graphite rod (diameter 20 mm, length 100 mm)	Spark observed, but the process cannot be called grinding.
4	Cathode: Wheel (bronze) thickness 5 mm Anode: Graphite block (140 mm × 100 mm × 20 mm)	No spark observed.
5	Cathode: Wheel (bronze) thickness 3 mm Anode: Graphite block (140 mm × 100 mm×20 mm)	Spark observed at the lower tool-electrode rotation range.

Table 2 Main parts of the experimental setup and their specifications/details

S. no.	*Name of parts*	*Specification/details*
1	Axial motion (x-, y- and z-direction)	Stepper motor (NEMA 23, step angle 1.8°, holding torque 19.1 kg.cm, phase current 2.8 A)
2	Tool attachment unit	Stepper motor (NEMA 17, step angle 1.8°, holding torque 4.2 kg.cm, phase current 1.7 A) and V-belt drive
3	Ball screw	Stainless steel (SFU2005, diameter ball screw rod 20 mm, pitch 5 mm, ball diameter 3.175 mm)
4	Table travel	x-axis (200 mm), y-axis (50 mm)
5	Machining chamber	Acrylic (360 mm × 250 mm × 150 mm)
6	Tool electrodes	Grinding wheel
7	Anode	Graphite block (140 mm × 100 mm × 20 mm)

A separate DC power supply unit is provided to operate stepper motor controller unit. The micro-stepping drivers (Rhino Motion Controllers) provided smooth operation to stepper motor. This micro-stepping drive was connected to a microcontroller board. Arduino Uno was selected as microcontroller board, and the programming was done on Arduino IDE. The exhaust fan was provided to extract the heat of the controllers.

Table 3 The specification/details of electrical and electronic units

S. no.	*Electrical and electronics unit*	*Specification/details*
1	Power supply unit	Pulse DC power supply: supply voltage (1–100 V), pulse-on time (1-9,999 μs), pulse-off time (1–9,999 μs), electric current (1–3 A)
2	Microcontroller board	Arduino Uno
3	Micro-stepping driver	Rhino motion controllers (RMCS-1102)
4	Laptop	Window 10

3.3 Machine user interface

The user interface or machine user interface is part of the machine that manipulates the user's command in a format that can be easily understood by the machine. GRBL firmware that runs on Arduino program to convert G-code commands to the stepper motor rotation.

4 Materials and methods

Alumina-reinforced-epoxy-nanocomposite (ARENC) is chemically inert electrically non-conductive material. The workpiece specimens were prepared in laboratory (Kadhim et al., 2013). Initially, the moisture from alumina nanoparticles was removed. Then, weighed epoxy and nanoparticles and methyl ethyl ketone (MEK) were mixed, and the weight of the mixture was noted. The mixture was placed on the magnetic stirrer for 700 rpm at 85°C for 2 hours for mixing. The weight of the mixture was continuously monitored. MEK evaporates with time, and the mixture was left with alumina nanoparticles and epoxy resin. When MEK completely evaporated, the mixture was placed again on the magnetic stirrer at same rpm but room temperature. When the temperature of mixture came down to room temperature, hardener was added to it, and mixed by glass rod manually. The mixture was poured into mould and left for 24 hours at room temperature. Then, the samples of rectangular plate (85 mm × 20 mm × 3 mm) were cut from prepared samples as shown in Figure 6.

The experiments were conducted on indigenously developed experimental setup of ECDPSG process based on OPAT. During the experimentation, some of the process parameters were fixed at a value. The experimental details for fixed process parameters are shown in Table 4.

In present work, Aq. NaOH was selected as electrolyte medium (Jawalkar et al., 2014). The input process parameters and its ranges were selected based on preliminary experiments. The low levels of the input process parameters were decided at a value, where observed spark was sufficient enough to melt and evaporate the workpiece material. The higher limits of the input process parameters are decided at a value up to which quality of machined surface maintained. Beyond this higher limit, quality of machined surface starts to degrade, also, at higher level of input process parameters, thermal cracks, fumes generation are observed.

Figure 6 Line diagram and photographic view of prepared sample for experimentation

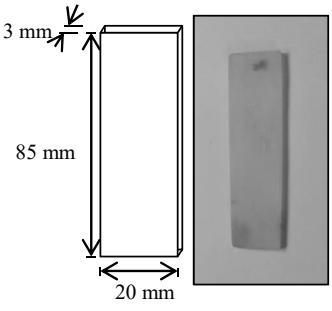

Table 4 Experimental details for fixed process parameters

S. no.	*Fixed process parameters*	*Symbol*	*Values*
1	Table feed rate (in x-direction) (mm/min)	f_w	0.5
2	Inter electrode gap (mm)		50
3	Pulse-off time (µs)	T_{OFF}	500
4	Electrolyte		Aq. NaOH
5	Tool electrode type		Grinding wheel (specification: D80/100M100M3/16, inner diameter 16 mm, outer diameter 70 mm (including abrasive layer thickness 10 mm), disc thickness 3 mm)

For present experimental parametric study, supply voltage, electrolyte concentration, pulse-on time and wheel rotation were selected as input process parameters to understand each aspect of machining process, e.g., supply voltage and pulse-on time are related to electric unit, wheel rotation is related to mechanical unit of machine, and electrolyte concentration is related to machining media.

The range of supply voltage was decided 55 V–65 V because below supply voltage 55 V, the observed spark was not capable for melting the workpiece material. When supply voltage was increased beyond 65 V, thermal cracks were observed on the workpiece. Pulse-on time was decided 1,000 µs–3,000 µs, because the presence of relative motion between immersed peripheral surface of wheel and electrolyte affects the hydrogen gas bubble generation rate and slows down the gas film formation around dipped surface area of metallic disc. Therefore, voltage is required to supply for larger time duration. Hence, lower value of pulse-on time was selected 1,000 µs. However, when pulse-on time was increased beyond 3,000 µs, spark interaction time increased, which resulted poor quality machined surface.

Electrolyte concentration was selected 100 g/l to 300 g/l because at electrolyte concentration below 100 g/l, observed spark was not prominent enough to cause melting of the workpiece surface. However, when the electrolyte concentration was taken beyond 300 g/l, the temperature of electrolyte increased rapidly during machining and toxic fumes were produced when spark was generated. Therefore, maximum limit of electrolyte concentration was selected 300 g/l.

A range of the wheel rotation speed from 3 rpm to 5 rpm was selected, which results the wheel peripheral speed (v_p) from 0.6597 m/min to 1.0995 m/min ($v_p = \pi DN_S$), respectively. During preliminary experiments it was observed that below 3 rpm, spark observed but molten material of workpiece (debris particles) present in between the wheel-workpiece gap were not flushed out from the sparking zone, and most of the thermal energy of the sparks was wasted. Therefore, lower limit of wheel rotation was selected as 3 rpm. However, when wheel rotation was increased beyond 5 rpm, the gas film becomes unstable, and observed sparks did not have sufficient energy to melt the workpiece surface. With increase in wheel rotation, electrochemical discharge phenomenon diminishes due to inability in adherence of hydrogen bubbles to wheel periphery. Hence, abrasion becomes main mechanism for material removal.

MRR indicates efficiency of the process, and R_a indicates quality of the machined surface. Therefore, for an efficient machining process, performance parameters MRR and R_a were selected.

Table 5 shows the experimental details for input process parameters and output performance parameters.

Each experiment has been repeated thrice to ensure the accuracy of the data. During the experimentation, the error can be due to uncontrollable factors such as atmospheric condition and human error. Therefore, the error bars are plotted in graphs to illustrate such errors.

Table 5 Experimental details for input process parameters and output performance parameters

Input process parameters	*Symbol*	*Values at different levels*		
Supply voltage (V)	V_S	55	60	65
Electrolyte concentration (g/l)	E_C	100	200	300
Pulse-on time (μs)	T_{ON}	1000	2000	3000
Wheel rotation (rpm)	N_S	3	4	5
Output performance parameters		*Symbol*		
Material removal rate (mg/min)		MRR		
Average surface roughness (μm)		Ra		

5 Results and discussion

The experiments were conducted on experimental setup of ECDPSG process based on a one-parameter-at-a-time (OPAT) approach. The graphs were plotted in Origin lab software. The effects of input process parameters on output performance parameters like MRR and R_a analysed based on these graphs, are discussed here:

5.1 Effect of supply voltage

Figure 7 shows the variation of MRR with supply voltage at different values of wheel rotations. Here, it is observed that when the supply voltage increases from 55 V to 65 V at wheel rotation 3 rpm, MRR increases by 547.66%. The electrochemical reactions occur between the bonding material of wheel and auxiliary electrodes. The evolution of hydrogen gas bubbles at the cathode occurs; the bubbles coalesce and form a gas film

around the bonding material and isolate the bonding material surface from electrolyte. On further increment of the supply voltage, the potential difference between the electrodes increases; this results in intensified sparks generation across the gas film. Thus, more discharge energy is generated at the bonding material surface of disc and electrolyte interface. The workpiece is placed near the sparking zone; thus, more material is melted. During pulse-off time, this molten material is ejected from the melting zone. The trend of supply voltage with MRR remains the same for wheel rotation 4 rpm and 5 rpm.

Figure 7 Effect of the supply voltage (V_S) on MRR at (E_C = 100 g/l and T_{ON} = 1,000 µs) (see online version for colours)

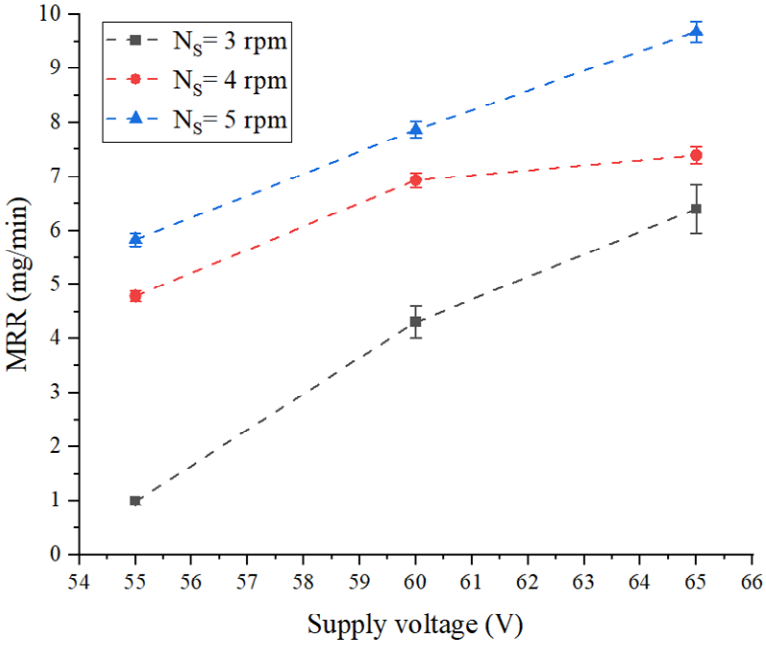

On comparing the values of MRR at wheel rotation 3 rpm, 4 rpm, and 5 rpm, at supply voltage 60 V, it was found that on increasing wheel rotation from 3 rpm to 5 rpm, MRR increases by 82.59%. This is so because on increasing N_S, the number of abrasives comes in contact with workpiece surface per minute increases. Hence, the material removed increases.

Figure 8 shows the effects of supply voltage on R_a. Here, it was observed that R_a is found to be increased by 121.21% due to an increase in supply voltage from 55 V to 65 V at wheel rotation 3 rpm. The thermal energy (Q) due to spark ($Q = V_S \times I \times T_{ON}$) increases with increase in supply voltage. Thus, more thermal energy is directed to the workpiece surface causing melting of the workpiece material. During the pulse-off time, the molten material can be either ejected completely or re-solidified. In case of complete ejection, the deeper craters are formed; in later case, re-solidified material is unevenly distributed over the machined surface leading to increase in R_a. In both of the mentioned cases, average surface roughness increases. However, on increasing wheel rotation, R_a initially increases then reduces. This is because when wheel rotation increases from 3 rpm to 4 rpm, the material removal due to electrochemical discharge phenomenon

dominates and the material is removed due to melting and vaporisation or melting and ejection. However, with increase in wheel rotation, it becomes difficult for gas bubbles to adhere on the periphery of wheel. Hence, abrasion participates actively for removal of re-solidified material over the machined surface, which leads to reduction in R_a.

Figure 8 Effect of the supply voltage (V_S) on R_a at (E_C = 100 g/l and T_{ON} = 1,000 µs) (see online version for colours)

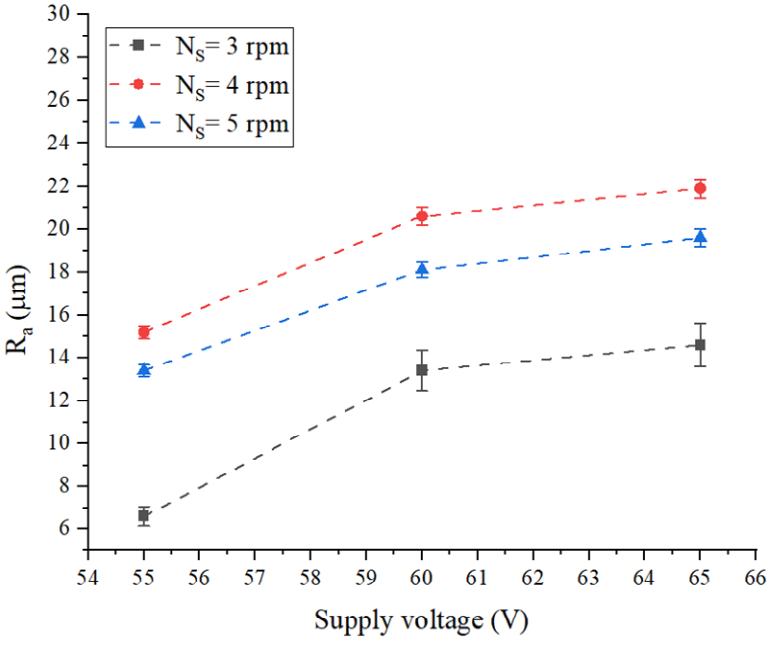

5.2 *Effect of pulse-on time*

Figure 9 shows the variation of MRR with pulse-on time. Here, it is observed that an increase of 579.46% in MRR is observed due to an increase in pulse-on time from 1,000 µs to 3,000 µs at wheel rotation 3 rpm. On increasing pulse-on time, there are two possibilities; first, when pulse-on time is more than gas film formation time, multiple sparks are generated; second, when pulse-on time is less than the gas film formation time, the sparking duration increases. In either case, the available total discharge energy increases, and more heat is available at machining zone. MRR increases with the increase in pulse-on time for a particular wheel rotation. Similar trend is followed for other wheel rotations.

Figure 10 shows the variation in R_a with pulse-on time. Here, it is noted that with an increase in pulse-on time, R_a increased by 90.91% at wheel rotation 3 rpm. On increasing pulse-on time, the heat available at machining zone increases as mentioned in earlier paragraph. Therefore, the material removal due to melting and vaporisation or melting and ejection is more than due to abrasion. Hence, R_a increases.

On the other hand, when wheel rotation is increases the material removed due to melting and vaporisation or melting and ejection reduces. Also, re-solidified material due to incomplete ejection was removed by abrasion. Therefore, R_a reduces.

Figure 9 Effect of pulse-on time (T_{ON}) on MRR at (E_C = 100 g/l and V_S = 55 V) (see online version for colours)

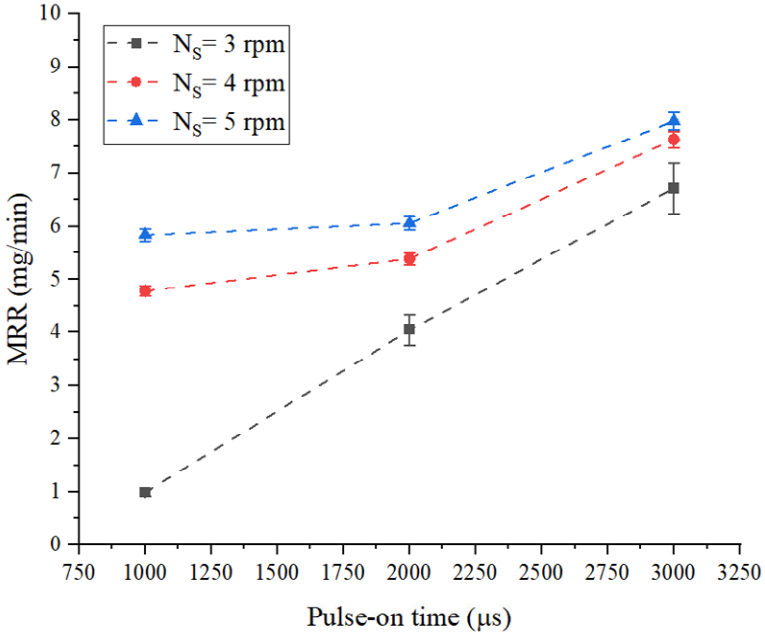

Figure 10 Effect of pulse-on time (T_{ON}) on R_a at (E_C = 100 g/l and V_S = 55 V) (see online version for colours)

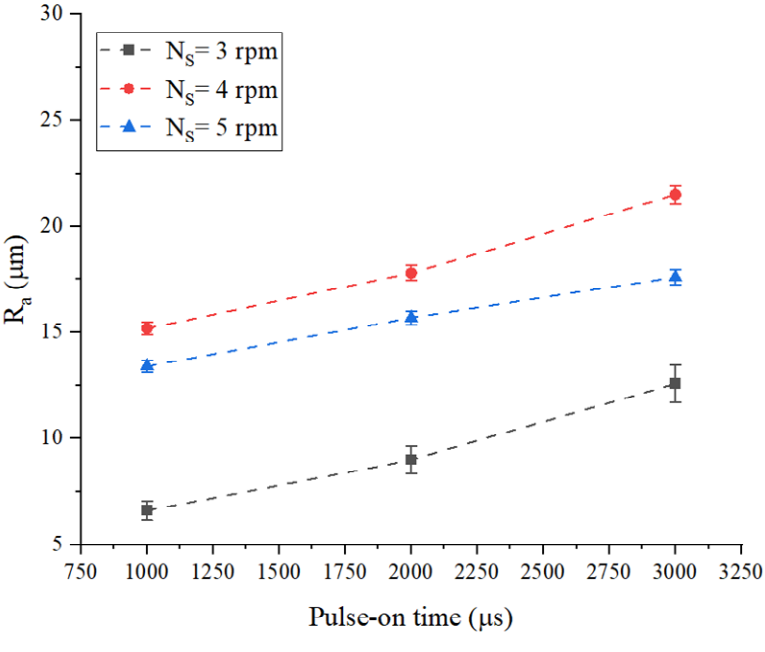

5.3 Effect of electrolyte concentration

In the case of grinding wheel, the bonding material is electrically conductive, and diamond abrasives are electrically non-conductive. The electrolyte concentration affects the electrolysis process.

Figure 11 Effect of electrolyte concentration (E_C) on MRR at (T_{ON} = 1,000 µs and V_S = 55 V) (see online version for colours)

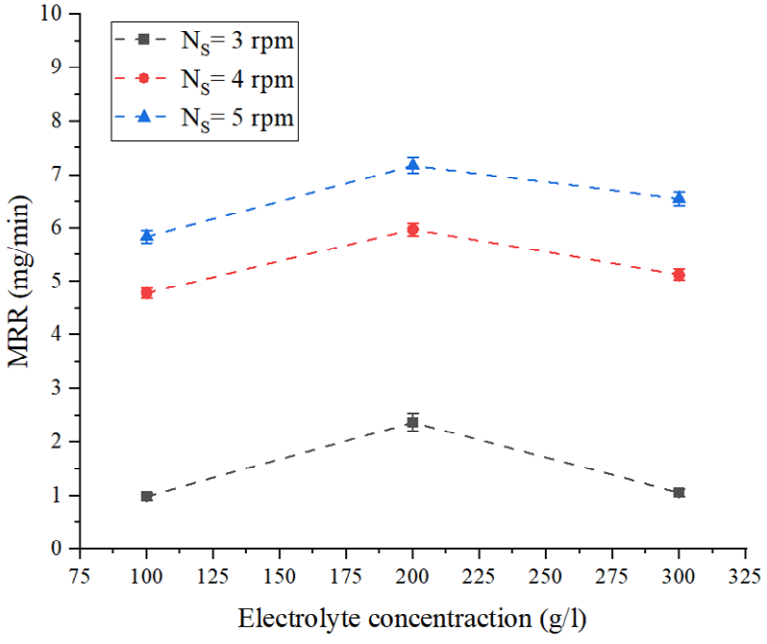

On increasing the electrolyte concentration from 100 g/l to 200 g/l, the electrolysis rate increases leading to the formation of hydrogen bubbles at the cathode. Hence, the gas film formation time reduces, and sparks are generated multiple times for the same pulse-on time. The multiple sparking at a place is responsible for a large sum of discharge energy at the workpiece surface and results in more melting of the superficial workpiece material. On increasing electrolyte concentration from 200 g/l to 300 g/l reduces the electrolysis rate while increasing gas film formation time. Thus, the number of electric sparks generated within the same pulse-on time also decreases. Therefore, initially, MRR increases by 140.04% with electrolyte up to 200 g/l, and then on the further increment of electrolyte concentration 300 g/l, MRR decreases by 55.46%. A similar pattern is observed for the effects of electrolyte concentration on MRR at wheel rotation 4 rpm and 5 rpm (Figure 11).

Figure 12 shows the effect of electrolyte concentration on R_a. Here, it is observed that at wheel rotation 3 rpm, when electrolyte concentration increases from 100 g/l to 200 g/l, R_a increases by 187.88% due to the effect of electrolyte concentration on electrolysis rate and gas film formation time. Therefore, multiple sparks can generate at the very same place on the workpiece surface. Therefore, the deeper craters are developed and cause an increase in R_a. Beyond electrolyte concentration 200 g/l, the electrolysis rate decreases, increasing gas film formation time. Therefore, fewer electric sparks are generated for the

same pulse-on time duration. Thus, less material is melted from the workpiece surface, and shallow craters are generated. Consequently, with an increase in electrolyte concentration from 200 g/l to 300 g/l, R_a reduces by 28.42%.

Figure 12 Effect of electrolyte concentration (E_C) on R_a at (T_{ON} = 1,000 µs and V_S = 55 V) (see online version for colours)

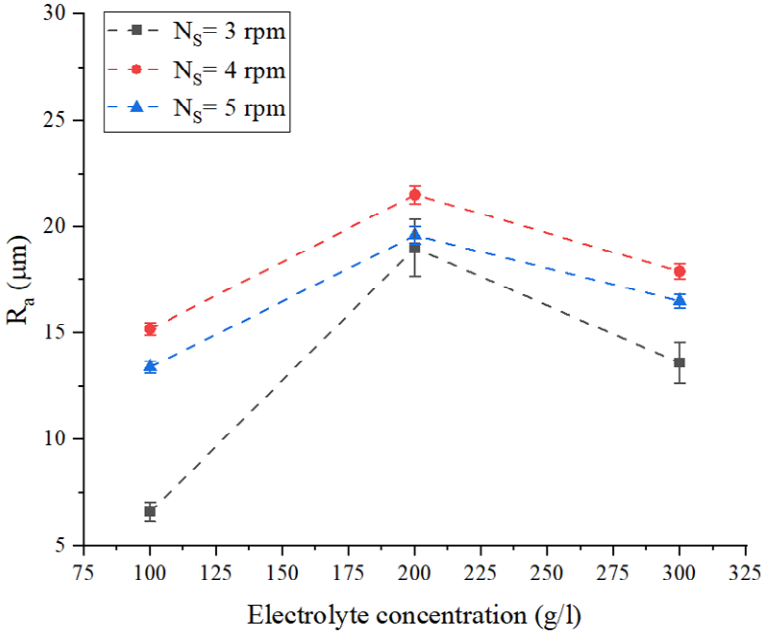

5.4 Effect of wheel rotation

Figures 13(a)–13(c) show the photographs of machined workpiece specimens using ECDPSG process at wheel rotation 3 rpm, 4 rpm and 5 rpm under the same experimental conditions. Here, the re-solidified material (which turned black after re-solidification) is kept on reducing while increasing wheel rotation. There can be three possible reasons behind this phenomenon; first, reduction in molten amount of material; second; that most of the amount of molten material is ejected; third, removal of re-solidified molten material by abrasion. Hence, all cases lead to increase in MRR while increasing wheel rotation.

On the other hand, increase in wheel rotation from 3 rpm to 4 rpm R_a increases. This is due the flushing efficiency of electrolyte is more at 4 rpm than at wheel rotation 3 rpm, therefore, the debris particles are easily flushed away from the machining zone. Thus, more thermal energy is directed to the workpiece surface causing melting of material. At pulse-off time, the molten material is ejected and crater is formed. On increasing wheel rotation from 4 rpm to 5 rpm, wheel peripheral speed is increased from 0.87962 m/min to 1.0995 m/min. Therefore, the effect of electrochemical discharge action reduces due to inability of adherence of gas bubbles at wheel peripheral surface, which further reduces

spark generation rate. However, effect of abrasion is increased as more number of abrasive grit per unit time at higher wheel rotation. Hence, abrasion action is responsible for removal of re-solidified molten material due to incomplete ejection. Hence, less number of craters with smooth machined surface is generated at comparatively higher wheel rotation, which reduces R_a.

Figure 13 Photographs of machined workpiece specimens using ECDPSG process at (a) N_S = 3 rpm, (b) N_S = 4 rpm, (c) N_S = 5 rpm, while keeping (V_S = 60 V, E_C = 100 g/l, and T_{ON} = 1,000 µs)

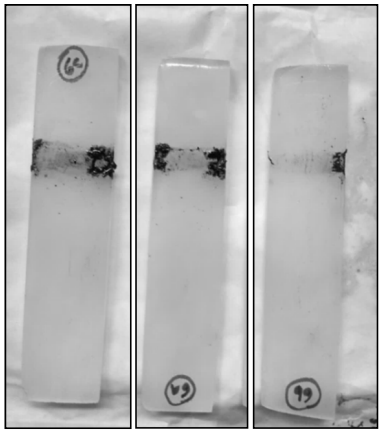

(a) (b) (c)

5.5 SEM analysis for ECDPSG process

Figure 14 shows the microscopic image of machined surface at 100 g/l electrolyte concentration. Here, it is noted that the crater boundary is uniform in depth. However in Figure 15 (machined surface at 200 g/l), the crater has non-uniform depth because along with the material removed from the channel, some extra nearby material is also melted and removed. This may be due to formation of gas film at edges of the wheel, which results in side sparking at the edges of wheel. Therefore, material removed at the corner of feature is shallow and superficial, which results uneven material removal from the workpiece surface. Figure 16 shows the machined surface having a channel-like shape at electrolyte concentration 300 g/l. Also, it has less material removed at the edges of feature, comparatively. This is because, beyond electrolyte concentration 200 g/l, the electrolysis rate decreases, increasing gas film formation time, which leads to decrease in available discharge energy for same pulse-on time. Therefore, R_a obtained at electrolyte concentration 300 g/l is slightly less than R_a obtained at electrolyte concentration 200 g/l. Therefore, R_a obtained at electrolyte concentration 300 g/l is slightly less than R_a obtained at electrolyte concentration 200 g/l.

Figure 14 Sample after ECDPSG process at V_S = 60 V, E_C = 100 g/l, T_{ON} = 1,000 µs, and N_S = 3 rpm

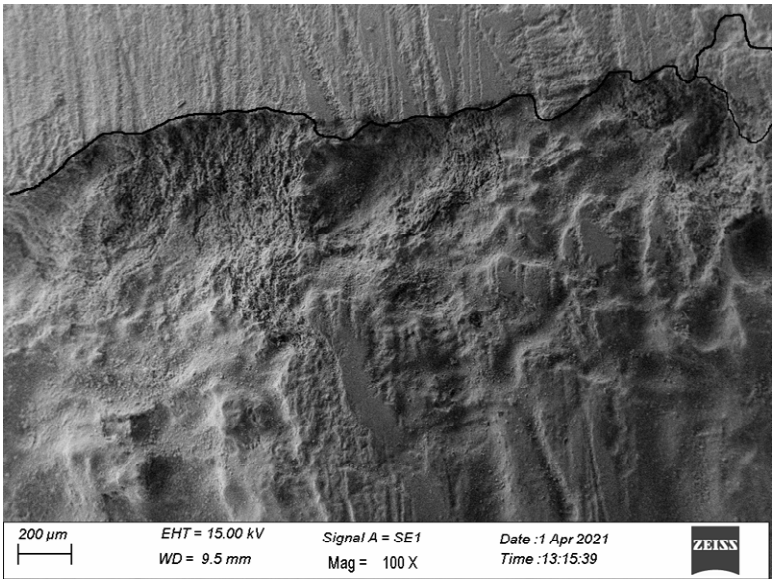

Figure 15 Sample after ECDPSG process at V_S = 60 V, E_C = 200 g/l, T_{ON} = 1,000 µs, and N_S = 3 rpm

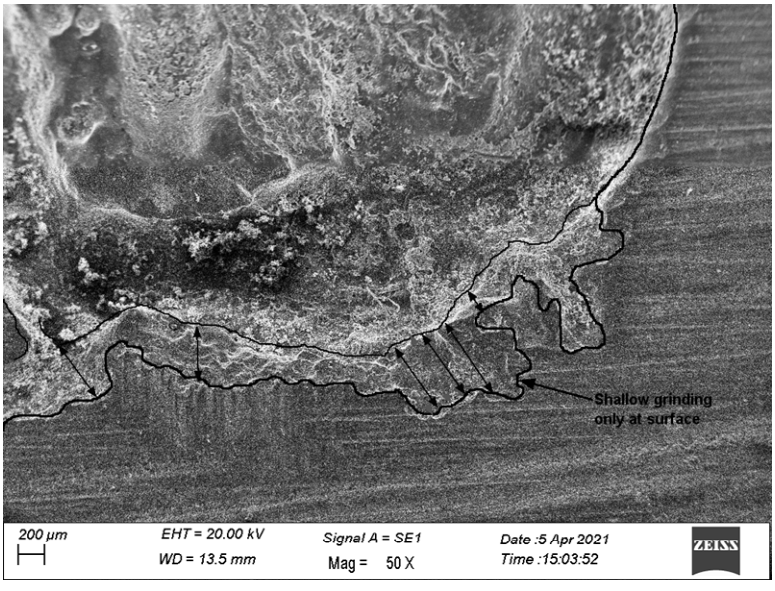

Figure 16 Sample after ECDPSG process at V_S = 60 V, E_C = 300 g/l, T_{ON} = 1,000 µs, and N_S = 3 rpm

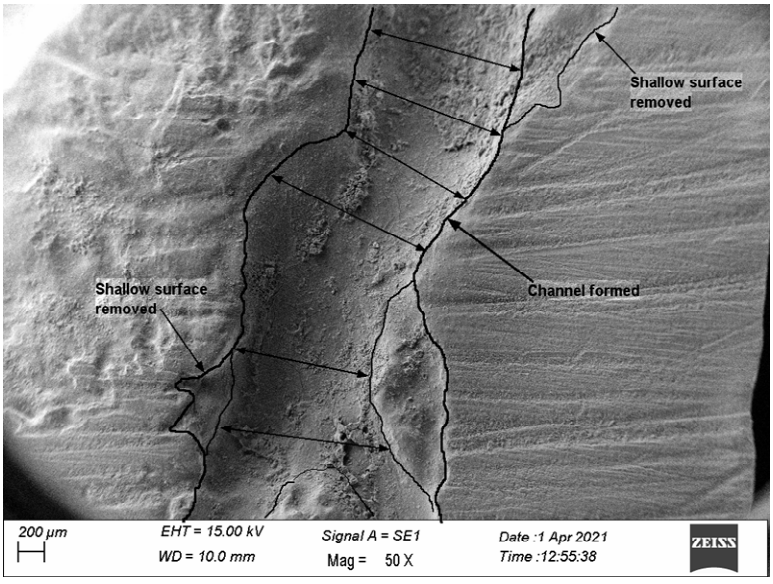

6 Conclusions

Experimental parametric studies for ECDPSG process were done for machining of electrically non-conductive ARENC workpiece specimens. The following conclusions have been drawn:

1 The experiments were carried out successfully on ARENC using ECDPSG process based on OPAT approach.

2 In ECDPSG process, the percentage increase in MRR (579.46% and 59.53%) on varying pulse-on time (T_{ON} = 1,000 µs to 3,000 µs) at wheel rotation (N_S = 3 rpm and 4 rpm) has been found highest. However, the percentage increase of MRR (65.92%) has been found highest for supply voltage (V_S = 55 V to 65 V) at wheel rotation (NS = 5 rpm). Hence, it can be concluded that at wheel rotation (N_S = 3 rpm and 4 rpm) pulse-on time is dominating whereas at higher wheel rotation, supply voltage is dominating input process parameter.

3 In ECDPSG process, the increase in R_a (121.21%, 44.08% and 46.27%) due to supply voltage (V_S = 55 V to 65 V) at wheel rotations (N_S = 3 rpm, 4 rpm and 5 rpm), which is the highest percentage increase in R_a. Therefore, it can be concluded that for R_a, supply voltage is dominating parameter regardless of wheel rotation condition.

4 After analysing the performance of the process, it can be concluded that the process has worked satisfactorily for electrically non-conductive materials. However, more studies like developing mathematical models, optimising the process, can be done in future to use the process in efficient and productive manner.

References

Ali, M.N., Doloi, B. and Sarkar, B.R. (2019) 'Electrochemical discharge machining technology applied for turning operation', in *IOP Conference Series: Materials Science and Engineering*, Vol. 65, p.012029.

Basak, I. and Ghosh, A. (1996) 'Mechanism of spark generation during electrochemical discharge machining: a theoretical model and experimental verification', *Journal of Materials Processing Technology*, Vol. 62, Nos. 1–3, pp.46–53, Elsevier.

Chak, S.K. and Venkateswara Rao, P. (2007) 'Trepanning of Al_2O_3 by electro-chemical discharge machining (ECDM) process using abrasive electrode with pulsed DC supply', *International Journal of Machine Tools and Manufacture*, Vol. 47, No. 14, pp.2061–2070.

Crichton, I.M. and McGeough, J.A. (1985) 'Studies of the discharge mechanisms in electrochemical arc machining', *Journal of Applied Electrochemistry*, Vol. 15, No. 1, pp.113–119.

Duncan, T.V. (2015) 'Release of engineered nanomaterials from polymer nanocomposites: the effect of matrix degradation', *ACS Applied Materials and Interfaces*, Vol. 7, No. 1, pp.20–39.

Fascio, V., Wüthrich, R. and Bleuler, H. (2004) 'Spark assisted chemical engraving in the light of electrochemistry', in *Electrochimica Acta*, Vol. 49, Nos. 22–23, pp. 3997–4003.

Fu, G. et al. (2022) 'Machinability investigation of polymer/GNP nanocomposites in micro-milling', *International Journal of Advanced Manufacturing Technology*, Vol. 119, Nos. 3–4, pp.2341–2353.

Hajian, M. et al. (2018) 'Experimental and numerical investigations of machining depth for glass material in electrochemical discharge milling', *Precision Engineering*, Vol. 51, No. 2018, pp.521–528.

Hussain, F. et al. (2006) 'Review article: polymer-matrix nanocomposites, processing, manufacturing, and application: an overview', *Journal of Composite Materials*, Vol. 40, No. 17, pp.1511–1575.

Jain, V.K., Dixit, P.M. and Pandey, P.M. (1999) 'On the analysis of the electrochemical spark machining process', *International Journal of Machine Tools and Manufacture*, Vol. 39, No. 1, pp.165–186.

Jawalkar, C.S., Sharma, A.K. and Kumar, P. (2014) 'Investigations on performance of ECDM process using NaOH and $NaNO_3$ electrolytes while micro machining soda lime glass', in *International Journal of Manufacturing Technology and Management*, Vol. 28, Nos. 1–3, pp.80–93.

Kadhim, M.J. et al. (2013) 'Microstructure and mechanical properties of Al_2O_3 matrix composite metal ceramic die materials', *International Journal of Application or Innovation in Engineering & Management (IJAIEM)*, Vol. 2, No. 11, pp.10–16.

Kulkarni, A., Sharan, R. and Lal, G. K. (2002) 'An experimental study of discharge mechanism in electrochemical discharge machining', *International Journal of Machine Tools and Manufacture*, Vol. 42, No. 10, pp.1121–1127.

Kurauchi, T. et al. (1991) 'Nylon 6-clay hybrid – synthesis, properties and application to automotive timing belt cover', *SAE Transactions*, Vol. 100, No. 5, pp.571–577.

Ladeesh, V.G. and Manu, R. (2018) 'Machining of fluidic channels on borosilicate glass using grinding-aided electrochemical discharge engraving (G-ECDE) and process optimization', *Journal of the Brazilian Society of Mechanical Sciences and Engineering*, Vol. 40, No. 6, p.299.

Liu, J.W., Yue, T.M. and Guo, Z.N. (2013) 'Grinding-aided electrochemical discharge machining of particulate reinforced metal matrix composites', *International Journal of Advanced Manufacturing Technology*, Vol. 68, Nos. 9–12, pp.2349–2357.

Nayak, R., Pradhan, M.K. and Sahoo, A. (2022) *Machinining of Nanocomposites*, 1st ed., CRC Press, Boca Ratan.

Singh, T., Arya, R.K. and Dvivedi, A. (2020) 'Experimental investigations into rotary mode electrochemical discharge drilling (RM-ECDD) of metal matrix composites', *Machining Science and Technology*, Vol. 24, No. 2, pp.195–226.

Starost, K. and Njuguna, J. (2014) 'A review on the effect of mechanical drilling on polymer nanocomposites – a review on the effect of mechanical drilling on polymer nanocomposites', in *IOP Conference Series: Materials Science and Engineering*, Vol. 64, p.012031.

Wan, Y. et al. (2008) 'Micro electro discharge machining of polymethylmethacrylate (PMMA)/multi-walled carbon nanotube (MWCNT) nanocomposites', *Advanced Composites Letters*, Vol. 17, No. 4, pp.115–123.

Wing, M.Y. et al. (2003) 'Polymer nanocomposites and their applications', *HKIE Transactions*, Vol. 10, No. 4, pp.67–73.

Wüthrich, R. and Bleuler, H. (2004) 'A model for electrode effects using percolation theory', *Electrochimica Acta*, Vol. 49, Nos. 9–10, pp.1547–1554.

Yadav, P., Yadava, V. and Narayan, A. (2018) 'Experimental investigation of kerf characteristics through wire electrochemical spark cutting of alumina epoxy nanocomposite', *Journal of Mechanical Science and Technology*, Vol. 32, No. 1, pp.345–350.

Yadav, P., Yadava, V. and Narayan, A. (2020) 'Experimental investigation for performance study of wire electrochemical spark cutting of silica epoxy nanocomposites', *Silicon*, Vol. 12, No. 5, pp.1023–1033.

Zhan, C. et al. (2017) 'Conductive polymer nanocomposites: a critical review of modern advanced devices', *Journal of Materials Chemistry C*, Vol. 5, No. 7, pp.1569–1585.